HVOF Coating Characterization by Acoustic Emission Using Four- Point Bending Test

S. Bouaricha, J.-G. Legoux and P. Marcoux
National Research Council Canada, Boucherville, Québec, Canada

Abstract

Four-point bend test using acoustic emission (AE) was used to compare coating properties under mechanical solicitation, mainly the toughness and the spalling behaviour. Coatings are made from the same material; the 2005NS (WC-17Co), sprayed with an HVOF gun at various spray parameters.

Coatings deposited on thin rectangular substrates were tested with the coating bent in tension and in compression. AE features like the event number, energy per event and cumulative energy were used to assess the damage in the coatings. The results are analyzed in relation with the coating microstructure.

Introduction

WC-Co-Cr and WC-Co coatings are largely used for wear resistance applications. Their behaviour under tests like erosion, abrasion and corrosion were treated in numerous publications. However, unlike TBCs [1-6], there are little studies dedicated to the evaluation of WC-based materials under mechanical solicitations such as the bend test coupled with acoustic emission [7-9].

This test could be a means of predicting deleterious failure phenomenon like spalling or delamination from substrate and by going back to thermal spray parameter set, determining which process parameters are influential.

The test consists in a four-point bending test, which allows monitoring the damage development on line. Indeed, it is performed by simultaneously applying a certain strain rate, measuring and analysing the characteristics of acoustic emissions. The formation of a crack during loading releases energy in the form of an acoustic wave, which propagates through the sample and may be detected using a piezoelectric sensor attached to the sample. Cracks are known to generally nucleate from defects, within and between splats or already were existed before bending.

In four-point bend evaluation, AE are burst type of event. Analyzing their features allows comparing between samples that present different mechanical behaviours due to their different microstructures.

In this study, we will try to correlate coating damage after bending and characteristics of acoustic emissions recorded during the mechanical solicitation.

Experimental Details and Set-up

Characterization

The diagnostic system DPV-2000 (Tecnar Automation) was used to measure the in-flight temperature, velocity and mean particle size during spraying.

Microhardness ($HV_{0.3}$) was measured from ten random indentations on the cross section of the coatings, with a load of 300 g and duration of 20 seconds.

The initial powder and coatings were examined using a Hitachi S-4700 scanning electron microscope (SEM). All deformed coatings were first infiltrated by epoxy to stabilize cracks generated by the bend test and to avoid creating new ones during cutting and polishing treatments. A polished longitudinal side plane between inner spans of the four-point bend test was observed.

X-ray diffraction measurements were carried out using a Bruker-AXS diffractometer with Cu-K_α radiation.

Residual stresses were evaluated from the curvatures of Almen strip type N.

Thermal Spraying

The starting material is the D-2005NS spray-dried and sintered powder from Sulzer-Metco, made of 83WC and 17Co in weight percentage as assessed by the manufacturer.

Coatings made from the D-2005NS powder were sprayed with the diamond Jet HVOF gun, using hydrogen as fuel and

Table 1: Sets of spray parameters used for the diamond Jet HVOF gun to produce samples # 1 to # 8.

Parameter	1	2	3	4	5	6			
Sample #	Ratio H_2/O_2	Total gas (l/min.)	SOD (cm)	Carrier gas N_2 (l/min.)	Substrate Surface T.(°C)	Thickness/ pass (µm)	H_2 (l/min.)	O_2 (l/min.)	Air (l/min.)
#1	2.4	2550	22.9	17.5	175	2.5	600	250	350
#2	2.4	2550	22.9	24	225	10.2	600	250	350
#3	2.4	2760	29.2	17.5	175	10.2	655	275	375
#4	2.4	2760	29.2	24	225	2.5	655	275	375
#5	3.6	2550	29.2	17.5	225	2.5	680	190	340
#6	3.6	2550	29.2	24	175	10.2	680	190	340
#7	3.6	2760	22.9	17.5	225	10.2	720	200	380
#8	3.6	2760	22.9	24	175	2.5	720	200	380

different sets of spray parameters. They were deposited onto grit-blasted mild steel substrates. Substrates have rectangular shape (Almen strip type N) with a size of 79.2 mm in length, 19.2 mm in width and about 1 mm in thickness.

Spray parameter sets are listed below in Table 1. They were defined to produce different coatings for further evaluation. An L-8 orthogonal array was used to produce coatings with eight sets of spray conditions. The effect of parameters was analysed using standard procedures for a Taguchi type matrix, based on DOE (design of experiments) techniques in order to find quantitative relationships, as described in a previous paper [10]. The following parameters were chosen as independent variables: H_2/O_2 ratio, total gas, spraying stand-off distance, carrier gas, substrate temperature and thickness per pass, and each parameter vary between two levels.

Four samples were produced for each spray parameter set. A special cylindrical shape sample-holder was designed to contain the four samples. During thermal spraying, the cylinder was rotated around its longitudinal axis, insuring to produce all the samples with similar thickness and substrate temperature.

Four-Point Bending Test

The four-point bending test set up was designed in our laboratory. The lengths of the inner and outer spans were 20.0 mm and 50.0 mm respectively. The motion of stress points is driven by a stepping motor power driver (from Klinger scientific corp.), which allows a continuous crosshead displacement rate as low as 50 µm/s. Thus, the bend test was run at a maximum deflection of 5 mm, which corresponds by calculus to about 1.2% strain in the tensile surface of the substrate and duration time of 100 s.

Tensile and compressive stresses were applied to the coating in such way that the deformation did not exceed the substrate elasticity limit. The 20 mm central region of the sample was in pure bending (constant bending moment and no shear forces).

Acoustic Emission

The acoustic emission (AE) signals were detected and picked-up using an acquisition board card NI5112 from National Instrument. Data acquisition was processed using a diagnostic apparatus developed in our laboratory and the post-test analysis was performed using a program built from LabView software (National Instrument).

Typically, an input AE signal that crosses a pre-set threshold level acts as a trigger signal. During testing, the acquired signals were preamplified and stored on the computer for subsequent data processing. Noise created by the testing machine and the specimen grips was eliminated by adequate filtering and threshold settings. Ultrasonic grease was used as a couplant between the sensor and the coupon. The sensor used was a piezoelectric of only 6 mm in diameter (panametrics, Mtl.) and sensitive to frequencies up to 1.5 MHz. The capture rate was set so that the time length saved for each digitized waveform was 2 ms, including a 0.2 ms pre-trigger before the waveform, to delineate the beginning of the waveform. The measurements of AE signals were representative after testing two to four samples.

Results and Discussion

Effect of Parameters on Temperature and Velocity

Average temperature and velocity profiles were calculated from the four profiles obtained with a parameter set at one level and were compared with the average profile for the same parameter set at its second level.

From figure 1 effects of H_2/O_2 ratio, total gas and carrier gas parameters on in-flight temperature and velocity of particles can be summarized as follows:

- At all stand-off distances, the increase in the stoichiometry (H_2/O_2 ratio) from 2.4 to 3.6 increases in-flight temperature but slightly decreases velocity.
- Increasing the total gas from 2550 to 2760 l/min. increases both temperature and velocity.
- The carrier gas has no effect on temperature and velocity when varied from 17.5 to 24 l/min.

Table 2 shows the in-flight temperature and velocity at stand-off distance, of particles for coatings #1 to #8, as defined earlier in Table 1. It also indicates the microhardness and the residual stresses obtained from curvature of Almen strips type N.

Microstructure Characterization

First of all, it is important to mention that all produced coatings presented a very low porosity, less than 1%. Thus, no discussion will be made on this point.

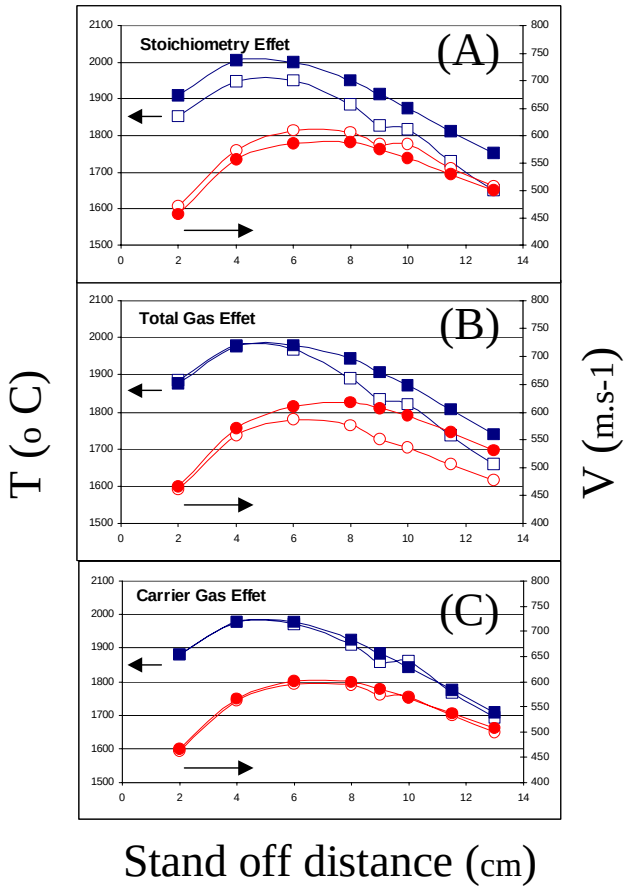

Figure 1: Effect of parameters on temperature and velocity. Square marks for temperature and circle marks for velocity. Open and full marks for lowest and highest levels, respectively, of the studied parameter as presented in Table 1.

Table 2: Temperature, velocity, microhardness and compressive residual stresses, normalized for similar thickness.

Sample	V (m/s)	T (°C)	H_v (kgf/mm^2)	Almen (μm)
#1	538	1746	1082.7	0.0111
#2	568	1804	1200.3	0.0421
#3	566	1754	1120.2	0.0099
#4	571	1794	1091.3	0.0112
#5	498	1795	1111.2	0.0077
#6	505	1775	1057.2	0.0055
#7	599	1923	1202.4	0.0128
#8	600	1943	1121.1	0.0096

Figure 2 shows microstructures for coatings #1 to #8, obtained by SEM. Characteristics of cracks regarding their density and morphology qualitatively represent all damages in the observed area.

None of the studied coatings spalled out or delaminated from their substrate. Indeed, all coatings exhibited clearly defined transversal cracks. Cracks can be seen to have propagated from the surface, normally to the load axis, to the coating-substrate interface without branches, then propagated parallelly along the interface. Defects within coating lead to stress concentrations and are believed to constitute the cracking origins. Also, It can be noted that cracks in all coatings were observed to be regularly spaced with distances varying from 0.4 to 1.1 mm. The average distance 'd' separating two cracks is reported in figure 2. Cracks formed in the coatings at regular intervals are consistent with the four-point bend test since the cracks will relieve the stress in a uniform manner. Depending on spray conditions, similar observations were already mentioned in numerous publications [6, 9, 11].

The width (opening) of transversal and interfacial cracks also varies with coatings. Indeed, coating # 5 has the largest cracks, followed by # 6, while coatings #1 and #7 exhibits the smallest crack opening.

X-ray diffraction patterns for coatings #1 to #8 were examined. They revealed that all coatings consist of WC as the major phase, with W_2C and W in small amounts resulting from the WC decarburisation. No clear peak related to the Co phase was found. On the other hand, all patterns show a broad diffraction halo at a range of $2\theta \approx [37,47°]$. This indicates the presence of a quantity of amorphous or nanocrystalline phase in each coating, probably composed of W, Co and C. Figure 3 shows an example of the X-ray diffraction patterns for coatings #2 and #3.

For all coatings, peaks related to W_2C and W phases are very small, which made their quantification difficult by a method like the Rietveld method for instance. However, it is possible by using other means, to get a way to relatively compare the amorphous fraction present in coatings. This is possible by using the index of crystallinity (I_c) as adopted by Verdon et al. [12]. The I_c is defined as the ratio between the areas of the Bragg peaks (crystalline material) and the total areas of the spectrum for 2θ comprised between 30 and 55 °. It gives relative proportions of crystalline and amorphous materials. Since one does not have the amorphous structure factor, values obtained for I_c are not absolute but can be used to rank the materials in a relative manner. Thus, the larger is I_c the more the coating is composed of crystalline material and undergone less carbide degradation. Table 3 shows the crystallinity index for all coatings. For example, it can be seen that coating #2 is less degraded than coating #3 (shown in figure 3), which is reflected by a higher portion of crystalline WC phase and I_c value.

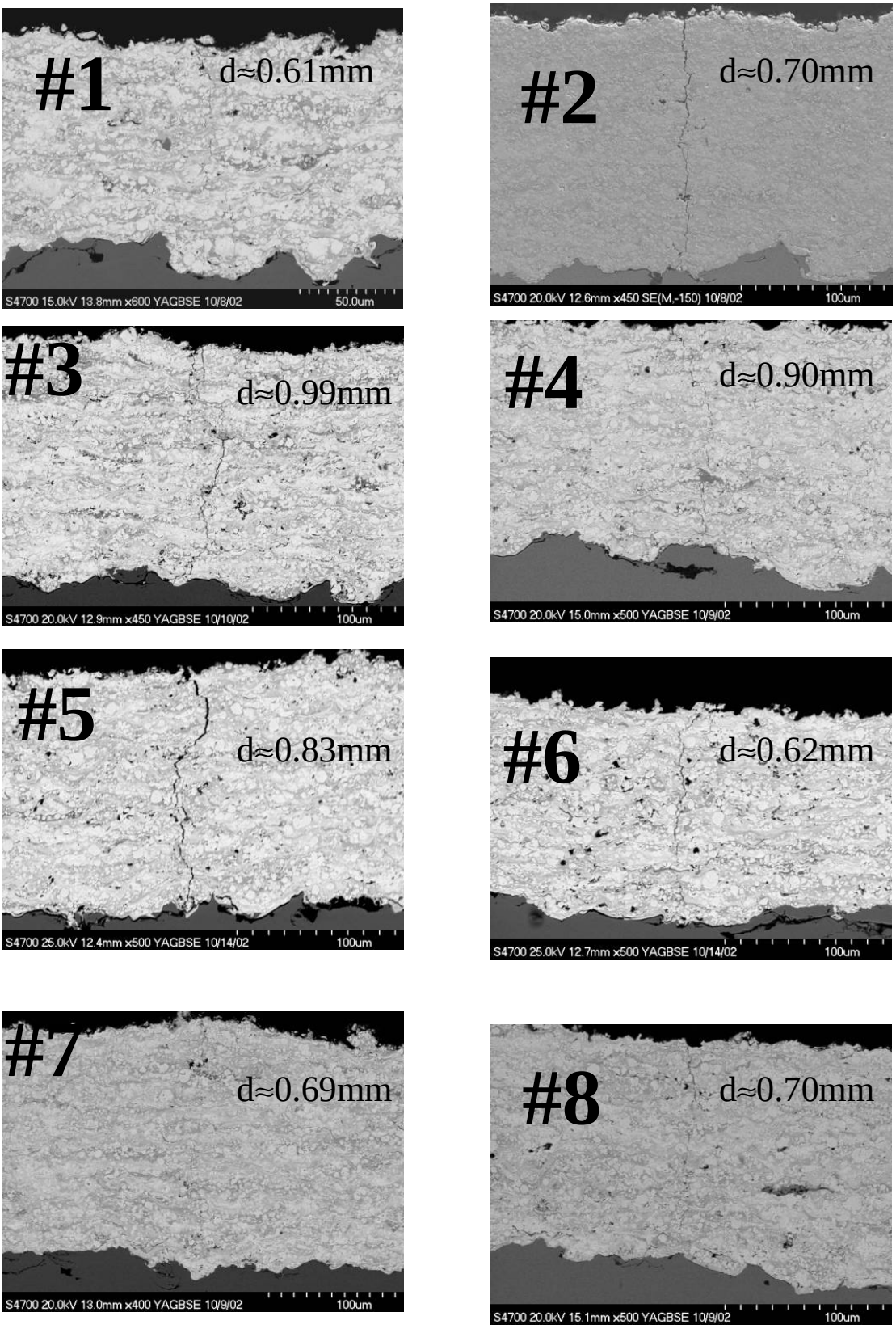

Figure 2: Cracks images for deformed coatings #1 to #8, obtained by SEM. 'd' is the average distance separating the transversal cracks.

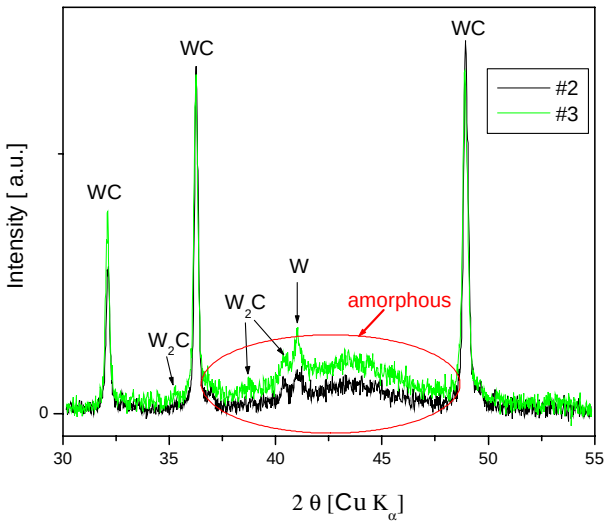

Figure 3: X-ray diffraction patterns of coatings #2 and #3.

Table 3: Indexes of crystallinity for coatings #1 to #8.

Sample Id	**#1**	**#2**	**#3**	**#4**
I_c	0,597	0,613	0.445	0.489
Sample Id	**#5**	**#6**	**#7**	**#8**
I_c	0.475	0.573	0.530	0.567

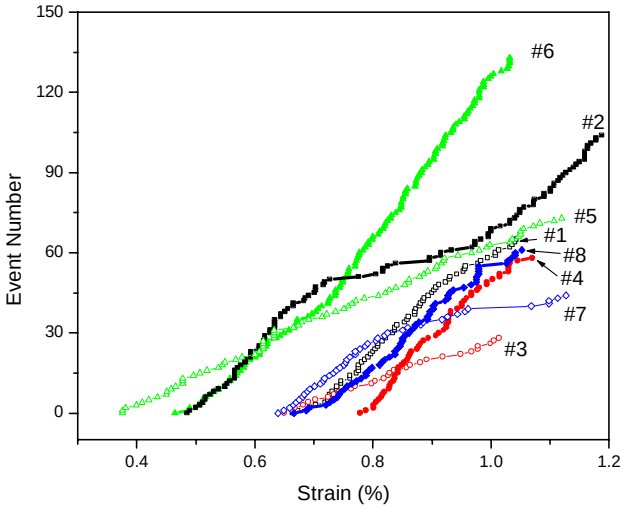

Figure 4: AE event number vs. strain.

Acoustic Emission Features

Figure 4 shows the number of event in function of strain recorded for bent coatings #1 to #8. The total number of events from the tests could distinguish the AE feature of either catastrophic failure or microcracking. As mentioned earlier, no catastrophic failure was produced in any of the coatings and this was perfectly measured by AE features, reflected by a continuous recording of AE events. Thus, from AE event number perspective, the coating damage mechanism is microcracking.

The first AE event corresponds to the onset of cracking,

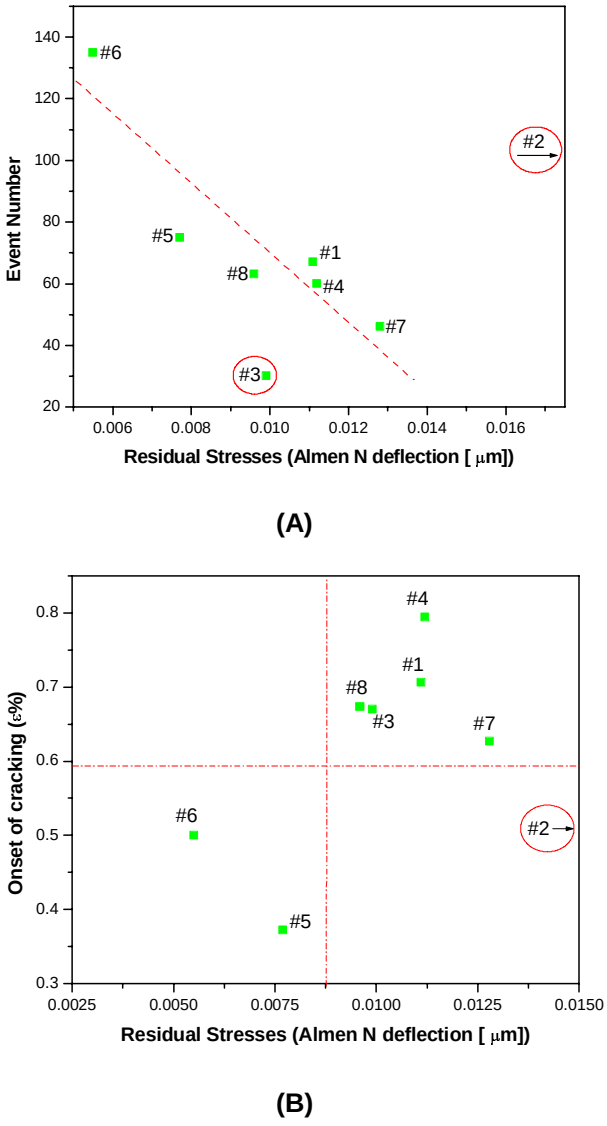

Figure 5: Residual stresses normalized for similar thickness vs. (A) AE event number and (B) onset of cracking.

coatings #5, #6 and #2 had the earliest crack initiation occurrence. This means that these coatings require less strain to initiate cracking. They also exhibit, overall the bending test, a much larger number of event than the other coatings. Figure 5A shows the event number plotted in function of residual stresses normalized for similar thickness. Of the eight points

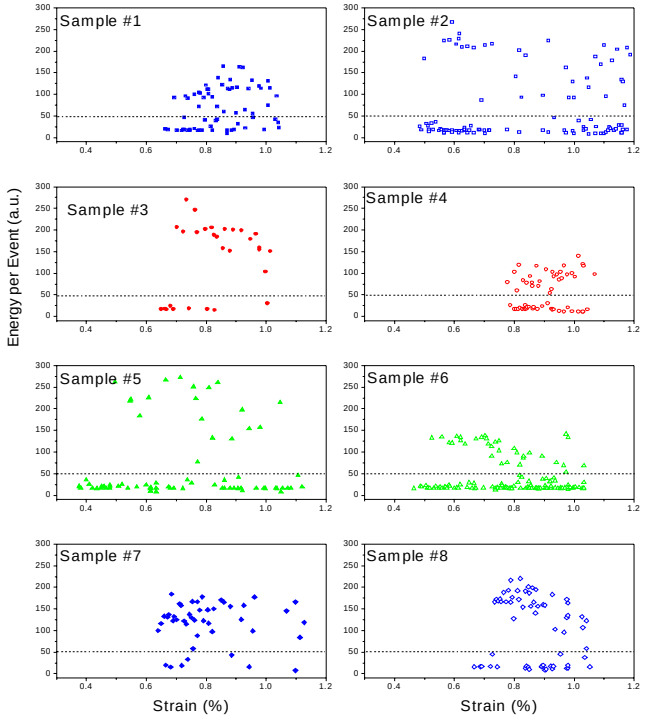

Figure 6: AE energy of events vs. strain.

plotted, six fall on a straight line, which suggest a relationship between them. We noted earlier that coatings that have initiated cracking first, presented the highest number of event. On this basis and regarding the linearity between event number and residual stresses, one could be attempted to link, by a transitive way through the event number, the onset of cracking and residual stresses. Figure 5B shows the onset of cracking vs. residual stresses. Unfortunately, it does not show a clear relationship between them, implying that other factors may play roles. Nevertheless, in the event of this being true, it suggests that delaying the initiation of cracking could be achieved by spraying coatings that present higher compressive residual stress values. However, caution must be made on this point and more work has to be done to verify this hypothesis.

Each coating exhibited events of different characteristics. The distinction between them, being weak or strong event, is expressed by the released acoustic energy. Figure 6 reports the energy of each event as a function of strain, recorded for coatings #1 to #8. The energy of an event is defined from the signal envelope. It can be seen that all coatings could be easily separated in two energy distributions, lower and higher than 50 a.u., as delimited by dotted lines. Dalmas et al. [9] have also observed, for coatings made from WC-Co, two different types of acoustic events in term of energy. In basis of microscopic observations, they attributed low absolute energy to transversal macrocracks and high energy to delamination. In our study, we do not have any proof that contradicts such attributions. On the contrary, these distributions illustrate

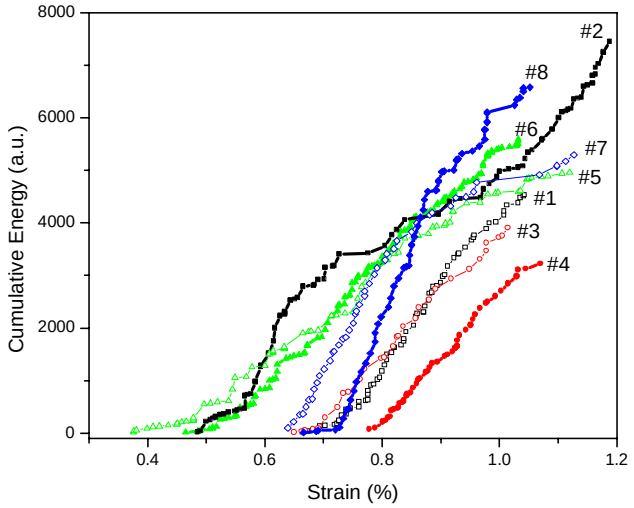

Figure 7: AE cumulative energy vs. strain.

clearly that weak and strong events alternate during all the range of applied strain, which corroborates the energy attribution made by Dalmas. One can also add that strong events are not generated only when approaching final failure, as showed by Lin et al. [13] for plasma sprayed TBCs. This confirms the damage mechanism by microcracking.

Although a coating can develop a large number of very small cracks, they could be not dangerous to its integrity; on the other hand it can develop a few large cracks that could be deleterious. Therefore, the analysis of the extent of damage is better described with the AE cumulative energy. Figure 7 is a graph showing the cumulative energy vs. strain for the deformed coatings. The cumulative energy is defined as the sum of energy of all events. This time, coatings #2, #8, #6 and #7 present higher cumulative energy values than the rest of the coatings. They also present higher cumulative energy for strong events (as shown in Table 4). It seems clear that the total cumulative energy is driven by the cumulative energy of strong events, rather than weak events.

Correlations between Microstructure and AE Features

Since none of the eight coatings spalled out from the substrate, the differentiation between coatings will be made in terms of acoustic emission features, confirmed by damage extent from microstructures. Nevertheless, damage sustained by a coating has to be defined since it is application dependent. In coating applications for wear resistance purpose like corrosion or leaking for example, it is of primary importance to not have cracks that could expose the substrate, otherwise coatings do not play their intended corrosion or leak-barrier protections. With its ability to detect the occurrence of microcracking, the onset of cracking detected by acoustic emission could answer to this. Earlier, the onset of cracking has been relatively linked to residual stresses. Thus, in order to maximize the coating resistance to crack initiation, one has to choose thermal spray

parameter set that gives to coatings high compressive residual stresses.

If one would expect to estimate the remaining lifetime of a coating before spalling or delamination, or to determine the amount of damage accumulation, further investigations would have to be done in order to understand different correlations.

The examination of specimen surface during interrupted tests (low applied strain, not shown here) revealed that cracks initiated from the surface and then propagated towards the substrate. This is consistent with the fact that the tensile stresses would be greatest near the coating surface. Also, it seems that all cracks are not formed simultaneously; they are rather formed one after another. Indeed, we have observed in many coatings for which deformation was interrupted, that cracks had already propagated toward the substrate and along the interface, followed by another crack, which had also initiated from the surface and only propagated for a portion of the coating's thickness. This clearly indicates both the progressive formation of the cracks and their distribution along the sample length.

Detailed examinations of the of crack shape are shown in figure 2, where the largest crack openings were observed for coatings #5, #6, #2 and #3, and the smallest for #7, #1 and #4. Note that the large crack openings seem to correlate with highest mean energy per event for strong events (> 50 a.u.), as reported in Table 4. This is in conformity with results published by Brown et al. [14] where they also observed that large cracks produced high energy AE events. The crack opening is believed to become larger with increasing applied strain [15].

In addition, crack spacing was found to correlate with the total cumulative energy. Indeed, with the exception of coating #1, figure 8A shows linearity between these two parameters. Coatings exhibiting larger crack spacing present the lower total AE cumulative energy. According to Zhou et al. [11], toughness is proportional to the square root of the crack spacing, which is in our case the mean distance 'd' separating two successive cracks. Thus, we can already establish a ranking between coatings regarding their toughness, and on this basis, coatings #3, #4 and #5 are the toughest among the eight deformed coatings. They have, respectively, 0.99, 0.90 and 0.83 mm as separating distance 'd'. Those coatings also present lower AE cumulative energy values in Table 4: associating this AE feature to higher coating toughness can also be done.
In another approach, we pointed out earlier that during the thermal spray process, the WC phase that constitutes in majority all coatings, has undergone a decarburisation. Dependent on used thermal spray parameter set, the carbide's degradation generated different amount of amorphous phase. Indeed, figure 8B reports the total cumulative energy versus the index of crystallinity and illustrates dependence between the amount of formed amorphous material and the cumulative

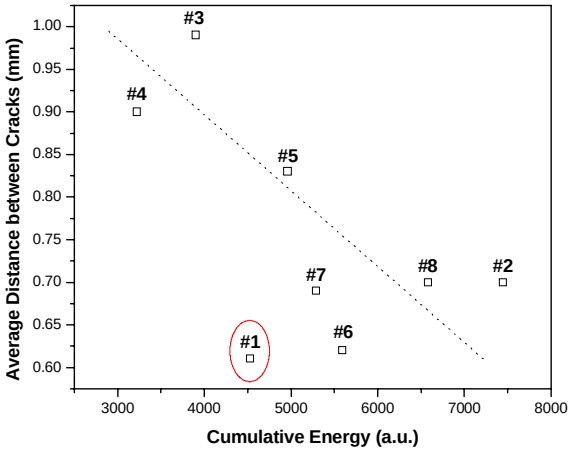

(A)

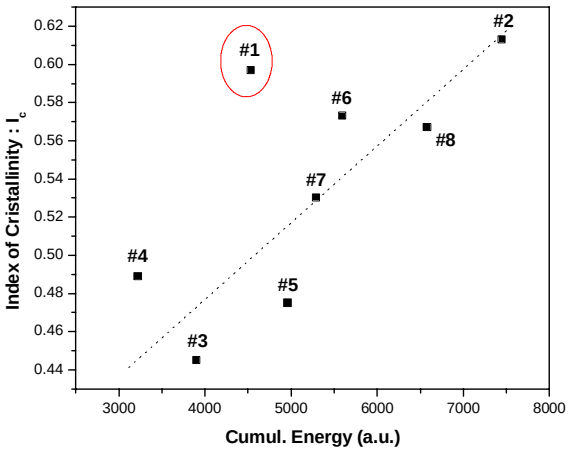

(B)

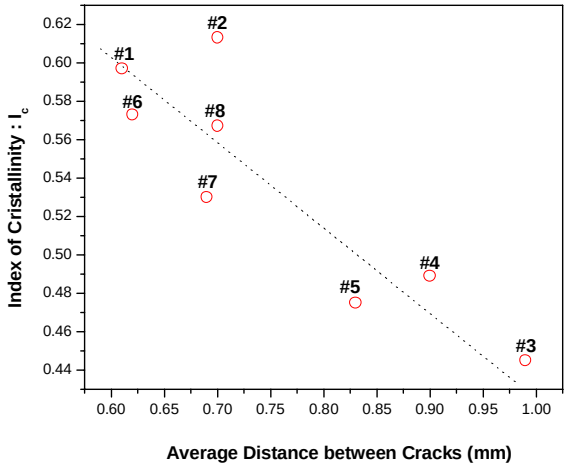

(C)

Figure 8: Relations between AE cumulative energy, average distance between cracks and index of crystallinity.

energy. The amorphous compound is known to be much softer than crystalline phases WC, W and W_2C. Subsequently, coatings that have the largest amount of amorphous material are the toughest ones. Moreover, figure 8C illustrates, in a transitive manner, the linear relationship between crack spacing and phase degradation from the I_C value.
We did not find any clear correlation between microhardness and AE features. One can say, as already reported by Cox [7]: *for applications where the toughness of a coating is of primary importance, hardness is probably not a reliable measure, but it is still valid as a quality control tool.*
Finally, it is noteworthy that the bending test of coatings in compression did not give reliable AE signatures. For all coatings, the few recorded AE event were of weak AE energy and a close look to their shapes shows that are likely formed from coating's slip rather than real AE generated by cracks.

Choice of Thermal Spray Parameter Set Based on AE Features
From above analysis, it seems that toughness is the key-characteristic to preserve coatings from failure by spalling or delamination. By going back to thermal spray parameter sets, we will determine which parameters influence the coatings toughness. Table 5 shows the effect of the chosen parameters on the AE features, as listed from the L-8 matrix conditions in Table 1. It can be summarized as follows:

- The spray distance influences the total cumulative energy, the AE cumulative energy of strong events and their event number, the index of crystallinity, the distance between cracks and the residual stresses.
- The total gas has an influence on mean energy per event, the cumulative energy for weak events as well as I_c and distance between cracks. The onset of cracking could be sensible to this parameter in spite of the relatively high interaction value.
- Surprisingly, the substrate temperature has no major effect.

Thus, mainly two parameters, the total gas and spray distance are affecting the AE features and the microstructure. The choice of the favourable thermal spray parameter set will be only based on how they influence favourably toughness through low AE cumulative energy.

Toughness vs. spray distance and total gas
As previously established, low AE cumulative energy is the

Table 4: AE features for all bent coatings.

Sample Idendity	**Onset of Cracking (ε%)**	**Event Number**	**Mean Energy per event (a.u.)**	**Cumul. Energ. (a.u.)**	**Event Number (< 50 a.u.)**	**Mean Energy per Event (< 50 a.u.)**	**Cumul. Energ. (< 50 a.u.)**	**Event Number (> 50 a.u.)**	**Mean Energy per Event (> 50 a.u.)**	**Cumul. Energ. (> 50 a.u.)**
#1	0.664	67	67	4533	30	24	710	37	103	3822
#2	0.485	106	70	7446	69	18	1259	37	167	6186
#3	0.65	30	130	3905	9	19	169	21	178	3736
#4	0.778	60	53	3223	30	18	528	30	90	2695
#5	0.376	75	66	4961	55	20	1079	20	194	3881
#6	0.465	135	41	5595	101	20	2021	33	108	3573
#7	0.639	46	115	5292	7	22	155	39	132	5137
#8	0.666	63	104	6581	24	19	447	39	157	6134

Table 5: Effect of parameters on AE features.

Property	**Ratio H_2/O_2**	**Total Gas**	**Spray Distance**	**Carrier Gas**	**Surf. Temp.**	**T/pass**	**Interaction**
Onset of Cracking	-0.29	-0.83	0.15	-0.06	0.35	0.34	0.51
Total Cumulative Energy	-830	883	1542	-1038	-77	-735	-1062
Mean Energy per event	-1.32	-39.47	16.48	27.28	9.64	-16.22	-23.29
Cumul. Energy of strong events	-567	-64	1840	-502	-163	-524	-1179
Mean Energy of Strong Event	-14	3	-2	22	-10	-11	-65
Number of events	-1.25	-0.25	11.75	-5.75	1.25	-0.75	5.25
Index of Cristallinity: I_c	-0.000250	0.05675	0.08125	-0.04875	0.01875	-0.00825	0.02225
Distances between cracks	0.09	-0.13	-0.16	0.05	-0.05	0.01	-0.1
Almen N Deflection	119	-50	129	0	-94	-14	-46

signature of coatings with high toughness. Thus, on ranking basis between coatings of low total cumulative energy and cumulative energy of strong events, as presented in Table 4, spraying at a SOD of 29.2 cm is more suitable than at 22.9 cm. Indeed, the four coating sets sprayed at 29.2 cm (#3, #4, #5 and #6. See Table 1) globally presented lower cumulative energy than the four coating sets sprayed at 22.9 cm (#1, #2, #7 and #8). This is in conformity to the work of Kucuk et al. [4], where they reported that coatings plasma sprayed at shorter SOD exhibited higher cracking activities. The SOD condition implies that particles should have a long residence time in the flame. Moreover, among the first set of coatings, coating #3 and #4 presented the lowest AE cumulative energy. As these two coatings used the highest level of total gas (i.e. 2760 l/min), it can be stated that (toughness wise) 2760 l/min of total gas is better than 2550 l/min.

Considering the chosen SOD's and total gas, and regarding the average particle in-flight temperature and velocity during spraying, higher total gas produces higher temperatures and velocities independently of both SODs (figure 1). Microstructures showed that at higher total gas, coatings undergone more carbide degradation. This could be interpreted by the fact that the increase in velocity does not sufficiently reduce the Dwell time to overcome the effect of the temperature.

Conclusion

For all coatings, no delamination or spalling was occurred. Instead, a network of regularly spaced parallel cracks, was observed along the surface of the coating and propagated toward the substrate and along the interface. Also of importance is the fact that no catastrophic failure occurred. Microcracking would therefore be the mechanism leading to failure of the coatings, which could make planned inspection by NDE a reliable means of monitoring the integrity of coated components.

This study proved the ability of AE to differentiate between coatings sprayed under different thermal spray conditions. Indeed, detailed investigations showed that coatings with higher compressive residual stresses seem have a higher resistance to crack initiation. This point has to be confirmed by adequately measuring the residual stresses with more reliable methods than the curvature of Almen, like the X-ray or the removal layer, for example. Regarding the damage extent observed and measured from the microstructure, the AE event number and cumulative energy are parameters describing with enough reliability the coating's cracking activity. In particular, distances separating cracks seems to apparently indicate the level of toughness in coatings. Also, it seems that the presence of more amorphous fraction in a coating plays a role in enhancing the toughness.

Acknowledgements

Thanks to Jan Wigren from Volvo for exchanging information regarding the bend test. Thanks to B. Harvey for software programming, to F. Belval for HVOF spraying, to M. Lamontagne for DPV-2000 measurements, to Éric Poirier for metallography and M. Thibodeau for SEM images.

Literature

1. Lin C.-K., C. C. Berndt, S.-H. Leigh and K. Murakami. J. Am. Ceram. Soc. 80, 3 (1997), pp. 2382-94.
2. Voyer J., F. Gitzhofer and M. I. Boulos. Journal of Thermal Spray Technology. 7, 2 (1998), pp. 181-190.
3. Kucuk A., C. C. Berndt, U. Senturk, R. S. Lima and C. R. C. Lima. Materials Science and Engineering. A284 (2000), pp. 29-40.
4. Kucuk A., C. C. Berndt, U. Senturk, and R. S. Lima. Materials Science and Engineering. A284 (2000), pp. 41-50.
5. Robin P., F. Gitzhofer and M. I. Boulos. Thermal Spary 2001: New Surfaces for a New Millenium. 28-30 May 2001. pp. 1247-1253.
6. Kucuk A., C. G. Dambra and C. C. Berndt. Practical Failure Analysis. 1, 1 February (2001), pp. 55-64.
7. Cox L. C. Surface and Coatings Technology, 36 (1988), pp. 807-815.
8. Richard C. S., G. Béranger, J. Lu, J.-F. Flavenot and T. Grégoire. Surface and Coatings Technology 78 (1996), pp. 284-294.
9. Dalmas D., S. Benmedakhene, C. Richard, A. Laksimi. Proceeding of the first ITSC, (2000), pp.1335-1340.
10. Legoux. J.-G. and S. Bouaricha. Proceeding of ITSC, Essen 2002, pp. 289-294.
11. Zhou Y. C., T. Tonomori, A. Yoshida, L. Liu, G. Bignall and T. Hashida. Surface and Coatings Technology (in press).
12. Verdon, C., A. Karimi and J.-L. Martin, Materials Science and Engineering A246 (1998), pp. 11-24.
13. Lin C.-K. and C. C. Berndt. Surface and coatings technology, 102 (1998), pp. 1-7.
14. Brown S. R. and I. G. Turner. Surface Engineering. 14, 4 (1998) 309-313.
15. Akita K., G. Zhang, S. Takahashi, H. Misawa H. and S. Tobe. Proceeding of the 15th International Thermal Spray Conference, Nice 1998, pp.837-842.